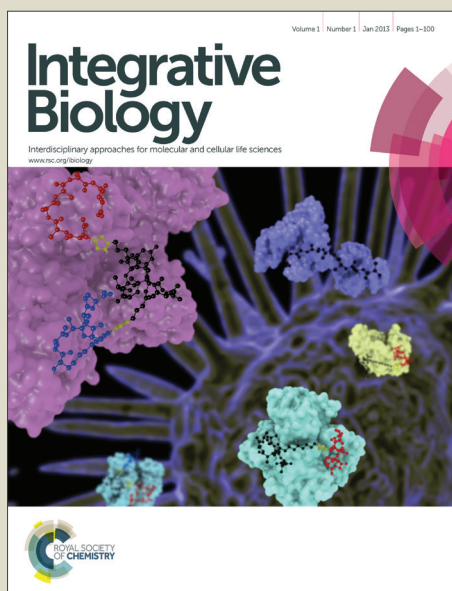


# Integrative Biology

Accepted Manuscript



This is an *Accepted Manuscript*, which has been through the Royal Society of Chemistry peer review process and has been accepted for publication.

*Accepted Manuscripts* are published online shortly after acceptance, before technical editing, formatting and proof reading. Using this free service, authors can make their results available to the community, in citable form, before we publish the edited article. We will replace this *Accepted Manuscript* with the edited and formatted *Advance Article* as soon as it is available.

You can find more information about *Accepted Manuscripts* in the [Information for Authors](#).

Please note that technical editing may introduce minor changes to the text and/or graphics, which may alter content. The journal's standard [Terms & Conditions](#) and the [Ethical guidelines](#) still apply. In no event shall the Royal Society of Chemistry be held responsible for any errors or omissions in this *Accepted Manuscript* or any consequences arising from the use of any information it contains.

## ARTICLE

## Organizational Metrics of Interchromatin Speckle Factor Domains: Integrative Classifier for Stem Cell Adhesion & Lineage Signaling

Cite this: DOI:

Received XX December 2014,

DOI: 10.1039/x0xx00000x

www.rsc.org/

Sebastián L. Vega<sup>#a</sup>, Anandika Dhaliwal<sup>#b</sup>, Varun Arvind<sup>b</sup>, Parth J Patel<sup>c</sup>, Nick R. M. Beijer<sup>d</sup>, Jan de Boer<sup>d,e</sup>, N. Sanjeeva Murthy<sup>f</sup>, Joachim Kohn<sup>f</sup>, Prabhas V. Moghe<sup>\*a,b</sup>

Stem cell fates on biomaterials are influenced by the complex confluence of microenvironmental cues emanating from soluble growth factors, cell-to-cell contacts, and biomaterial properties. Cell-microenvironment interactions influence the cell fate by initiating a series of outside-in signaling events that traverse from the focal adhesions to the nucleus via the cytoskeleton and modulate the sub-nuclear protein organization and gene expression. Here, we report a novel imaging-based framework that highlights the spatial organization of sub-nuclear proteins, specifically the splicing factor SC-35 in the nucleoplasm, as an *integrative marker* to distinguish between minute differences of stem cell lineage pathways in response to stimulatory soluble factors, surface topologies, and microscale topographies. This framework involves the high resolution image acquisition of SC-35 domains and imaging-based feature extraction to obtain quantitative nuclear metrics in tandem with machine learning approaches to generate a predictive cell state classification model. The acquired SC-35 metrics led to > 90% correct classification of emergent human mesenchymal stem cell (hMSC) phenotypes in populations of hMSCs exposed for merely 3 days to basal, adipogenic, or osteogenic soluble cues, as well as varying levels of dexamethasone-induced alkaline phosphatase (ALP) expression. Early osteogenic cellular responses across a series of surface patterns, fibrous scaffolds, and micropillars were also detected and classified using this imaging-based methodology. Complex cell states resulting from inhibition of RhoGTPase,  $\beta$ -catenin, and FAK could be classified with > 90% sensitivity on the basis of differences in the SC-35 organizational metrics. This indicates that SC-35 organization is sensitively impacted by adhesion-related signaling molecules that regulate osteogenic differentiation. Our results show that diverse microenvironment cues affect different attributes of the SC-35 organizational metrics and lead to distinct emergent organizational patterns. Taken together, these studies demonstrate that the early organization of SC-35 domains could serve as a "fingerprint" of the intracellular mechanotransductive signaling that governs growth factor- and topography-responsive stem cell states.

### Introduction

Human mesenchymal stem cells (hMSCs) are a multipotent autologous cell source with significant utility in regenerative therapies due to their *in-vitro* expansion and ability to differentiate into numerous connective tissues<sup>1, 2</sup>. Traditional strategies to direct hMSC differentiation towards one of the three mesodermal lineages (osteocytes, chondrocytes, and adipocytes) rely on the continuous induction by specific combinations of soluble growth factors<sup>2</sup>. More recently, stem

cell differentiation has been achieved by manipulating biomaterial properties, including substrate chemistry<sup>3</sup>, topography<sup>4, 5</sup>, and stiffness<sup>6, 7</sup>. Optimizing these microenvironmental cues is of particular interest in regenerative medicine where biomaterial substrates may serve as a vehicle for directed cell delivery or as a system for tissue formation *in-vivo*. Commonly used methods for assessing microenvironment modulated osteogenic and adipogenic differentiation include reverse transcriptase PCR (RT-PCR) for detection of osteogenic or adipogenic transcripts, immuno-histochemical

analysis, enzyme linked immunosorbent assay (ELISA) or western blotting for secreted protein markers, colorimetric assays, and direct staining of matrix components<sup>8,9</sup>. To aid in identifying optimal microenvironments that efficiently elicit strategic stem cell phenotypes, high-throughput screening (HTS) approaches that allow for the assessment of up to several thousand conditions within one experiment have also been developed<sup>10-12</sup>. However, these approaches rely on population-based phenotypic readouts. This is particularly problematic since: (1) these assays fail to capture the heterogeneity inherent to stem cell-derived cell populations, and (2) the markers being measured are not robustly expressed in stem cells unless they have differentiated, a process which can take several weeks to manifest. Consequently, these approaches are employed 14-40 days post differentiation induction<sup>13-16</sup>. Thus, a major need exists for the development of profiling tools to screen early phenotypic responses at the individual cell level and to forecast longer-term cell behaviors.

Adherent stem cells interact with their extracellular matrix through cell surface receptors, which propagate a cascade of signaling events to the cytoskeleton via focal adhesions, and ultimately to the nucleus. Previous studies have shown that the shape of the cell is a precursor to stem cell differentiation<sup>4,17,18</sup>. We propose the premise that the organization of subcellular proteins involved in outside-in signaling, particularly of those mediating mechanotransductive signaling, is regulated by microenvironmental cues during differentiation, and that these minute differences can be captured by enhanced content imaging. As a major evidence of this premise, our laboratory advanced an imaging-based profiling methodology that allows for the dissection of morphologic signatures in the cytoskeleton unique to a particular culture condition<sup>19-22</sup>. Using this approach, early (24 hour) actin morphologic signatures of hMSCs were identified and used to predict downstream osteogenic differentiation<sup>20</sup>. More recently, this technique was applied to distinguish between image-based features of nuclear mitotic apparatus (NuMA) protein organization of pluripotent versus spontaneously differentiating embryonic and induced pluripotent stem cells<sup>21</sup>. Although these studies have shown that stem cells adopt a higher-order organization of cytoskeletal and nuclear proteins (NuMA) that can be defined by shape, intensity, and texture descriptors, developing methods to discern stem cell states on more physiologic and complex biomaterial substrates and scaffolds remains a major challenge. In this study, we have proposed a new molecular reporter-based approach to profile cell states using more sensitive sub-nuclear signatures defined by a smaller set of descriptors.

Pajeroski et al. demonstrated that differentiating cells undergo progressive changes in gene expression, structural reorganization, and nuclear shape<sup>23</sup>. One of the goals of this study was to identify highly sensitive nuclear proteins as reporters to offer calibrated organizational features via high content imaging. To accomplish this, a number of candidate proteins within the nucleoskeletal scaffolding complexes were considered, namely RUNX2, Lamin A, trimethylated H3K4

histone (H3K4me3), EZH2, and SC-35. These sub-nuclear proteins have been implicated in microenvironment modulated

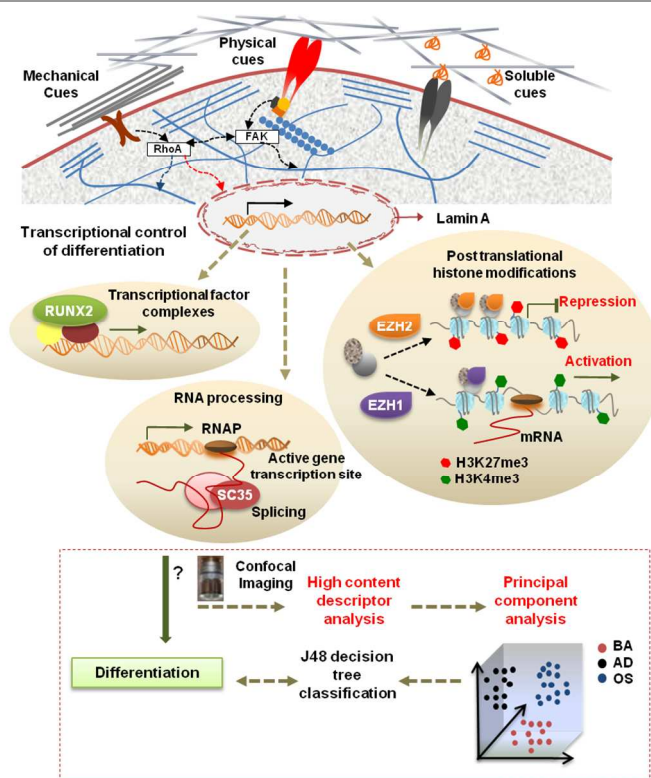


**Fig. 1: Workflow highlighting utility of nuclear imaging-based profiling.** Cell-material interactions modulate nuclear protein organization through signaling cascades as well as cytoskeletal-nuclear links, which regulates nuclear programs such as activation of transcriptional factors, posttranslational histone modifications, and RNA processing that direct gene expression and cell fate. In this study, the influences of microenvironmental cues on organization of various sub-nuclear reporters involved in these nuclear programs, namely, Lamin A, SC-35, RUNX2, H3K4me3, and EZH2 was evaluated at early time-points during differentiation. hMSCs were cultured on different substrates in the presence of adipogenic (AD) or osteogenic (OS) or basal media (BA) for 3 days, and high resolution images were acquired using confocal microscopy. High content analysis was then done to compute Haralick texture descriptors that define the spatial organization of the nuclear reporter. This set of descriptors was then dimensionally reduced using Principal Component Analysis (PCA). Subsequently, the principal components were taken as an input for a classifier that used machine-learning approaches based on a J48 decision tree algorithm to classify cells exposed to different conditions. The predictive classification model was validated by correlations with 14-day endpoint assays. Using this framework, we can go through several iterations to analyze changes in nuclear reporter organization and thus screen and identify microenvironmental cues that elicit desired phenotypic responses.

cell processes such as mechanotransduction, gene regulation, and stem cell differentiation (Fig. 1). EZH2 is a histone lysine methyltransferase that controls hMSC osteogenic differentiation via the trimethylation of H3K27<sup>24</sup>. Lamins are essential filaments of the nuclear envelope, and their presence (namely Lamin A) has been associated with preferential osteogenic differentiation in hMSCs<sup>25,26</sup>, while RUNX2 is a transcription factor that directly promotes osteogenic differentiation<sup>27</sup>. Upon methylation, H3K4me3 histone induces a transcriptionally active state for many genes involved in stem cell proliferation and differentiation<sup>28</sup>. SC-35 nuclear speckle domains host small nuclear ribonucleoprotein particles

(snRNPs)<sup>29</sup>, spliceosomes, and transcription factors that function in co-transcriptional modifications of RNA<sup>30</sup>.

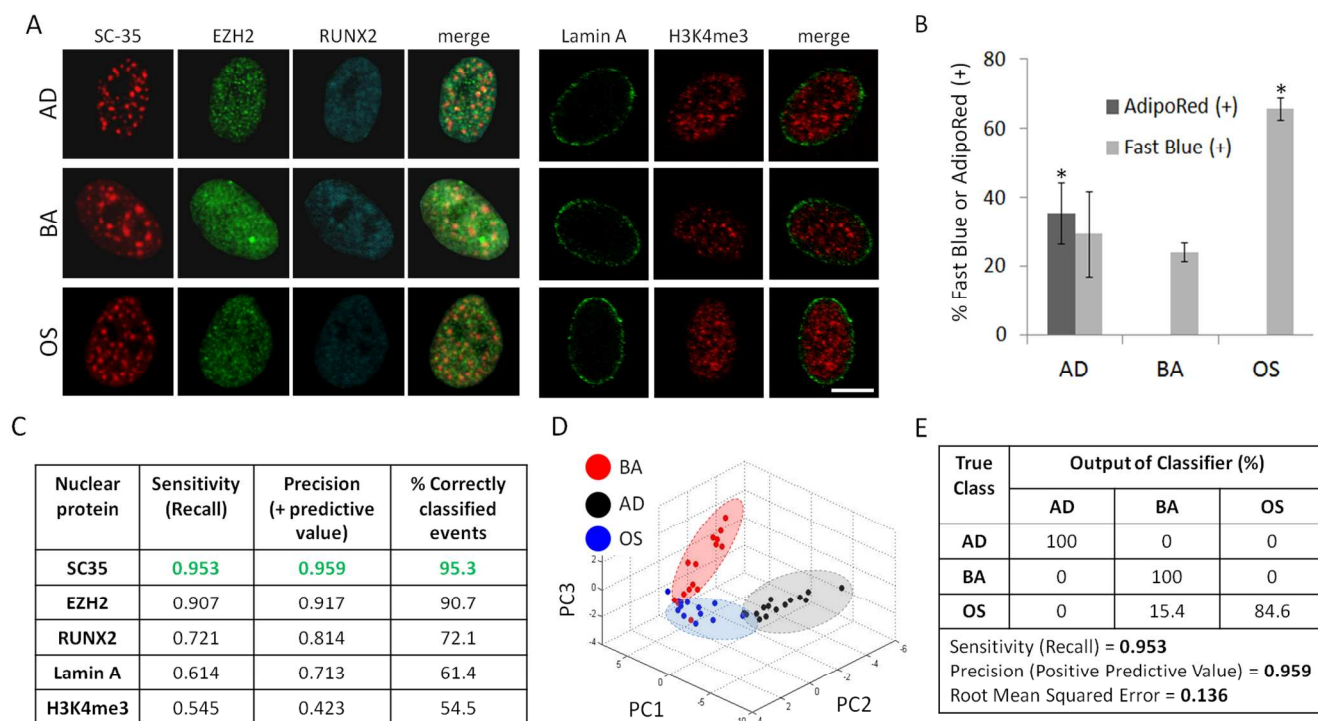


**Fig. 2: SC-35 organization as a screen to parse stem cell differentiation.** hMSCs were cultured in BA, AD, or OS media and **(A)** fixed and immunolabeled for a panel of either gene-modifying (H3K4me3, EZH2, RUNX2) or mechanoresponsive (Lamin A, SC-35) proteins 3 days post-plating. **(B)** hMSCs cultured in BA, AD, or OS media for 14 days were stained for intracellular triglycerides (AdipoRed) and alkaline phosphatase (ALP) to identify % of adipocytes and osteoblasts, respectively. **(C)** 3 day analysis of nuclear proteins yields differences in sensitivity, precision, and % of correctly classified events, and **(D)** PCA plot of SC-35 reporter shows that the three conditions cluster into three distinct groupings (blue = OS, black = AD, red = BA). **(E)** Decision tree analysis of PCA-derived principal components show that hMSCs parse well (> 95%). Scale bar = 5  $\mu$ m. \* indicates statistical significance ( $p < 0.01$ ). Sample size ranged from 13 to 15 cells per nuclear reporter per growth factor treatment condition.

In this study, we employed high content image acquisition of various nuclear proteins in tandem with machine learning modeling to evaluate single-cell responses of hMSCs to microenvironmental cues. hMSCs were cultured in different engineered microenvironments comprised of several topographies (i.e., patterns, fibers, micropillars) and soluble growth factors (**Fig. 1**). To identify potential structural changes of these reporters as a function of microenvironmental cues, high resolution images were subject to quantification by using Haralick texture features which resolve higher-order organizational features<sup>31</sup>. Based on neighboring pixel intensity within confocal images, 13 different Haralick texture features were computed (**Table S1**) using two different pixel groupings (termed C1, C2), resulting in 26 Haralick texture features in total, which were dimensionally reduced using PCA. The principal components were taken as inputs for a J48 decision tree classifier to create a classification model.

In the course of our screening of the panel of markers, we report that SC-35 is a highly responsive organizational reporter. We then focused subsequent experiments on investigating and validating the utility of SC-35 domain organization to predict osteogenic stem cell differentiation in hMSCs cultured across a series of more complex substrates, including surface patterns, fibrous scaffolds, and micropillar topographies.

## Results

### Nuclear proteins as a high content screen to parse stem cell differentiation

To screen for nuclear proteins whose early (3 day) organization is influenced by stem cell differentiation, hMSCs were cultured for 3 days and 14 days in either basal growth media (BA), adipogenic (AD), or osteogenic (OS) differentiation media prior to immunostaining for several nuclear reporters, namely H3K4me3, Lamin A, RUNX2, EZH2, and SC-35 (**Fig. 2A**).

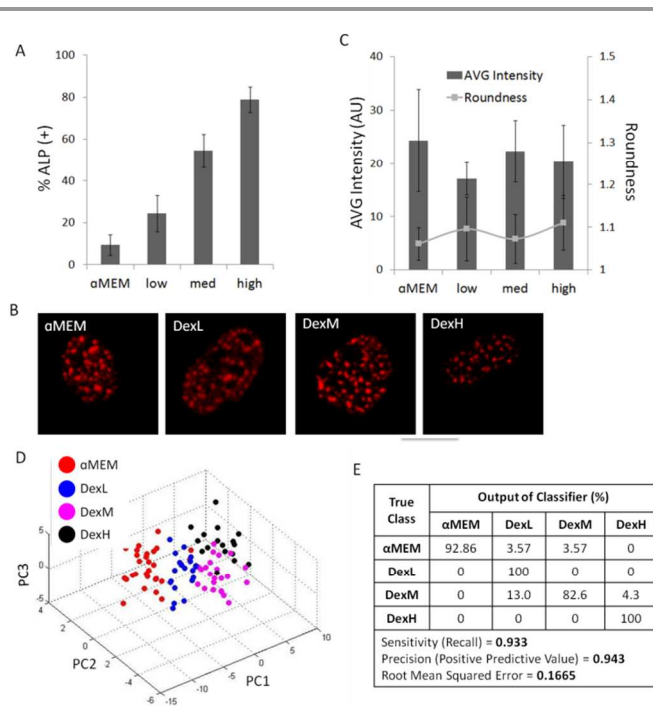


**Fig. 3: SC-35 domain descriptors distinguish dexamethasone-induced alkaline phosphatase expression within 3 days.** hMSCs were cultured in  $\alpha$ MEM supplemented with increasing levels of dexamethasone (*dex*) (low = 0.1  $\mu$ M, med = 0.5  $\mu$ M, high = 1  $\mu$ M), resulting in (A) an increasing percentage of alkaline phosphatase-positive cells after 14 days in culture. For % ALP determination at least 1,000 cells were counted for each condition. (B) Under the same culture conditions, representative SC-35 images and (C) average signal intensity of SC-35 (bars in plot) and nuclei roundness (dots in plot) are unable to discern differences between the different treatment groups at 3 days. However, 3 day analysis using 26 Haralick descriptors is capable of discerning differences between increasing *dex* conditions, confirmed by (D) distinct cluster formation in PCA plot and (E) decision tree analysis, which shows that 93% of cells can be correctly classified using our approach. For descriptor analysis, at least 40 cells were analysed for each condition.

The organization of the prescribed nuclear proteins was analyzed by performing a high content analysis on high resolution images obtained at 3 days wherein 26 Haralick texture descriptors were computed to define the organization. Independently, we confirmed that hMSCs cultured in AD media differentiated to adipocytes and stained positive for AdipoRed at 14 days, whereas AdipoRed was undetected in cells cultured in BA and OS culture conditions (Fig. 2B, S1). Additionally, hMSCs cultured in OS media exhibited osteogenic differentiation and had significantly more ( $p < 0.01$ ) fast blue staining as compared to cells cultured in BA and AD conditions for 14 days (Fig. 2B).

To identify differences in nuclear protein organization in response to growth factor induced differentiation, 26 numerical texture-based descriptor sets were computed after high content analysis for each nuclear protein within each condition. Principal component analysis (PCA) was then performed to dimensionally reduce the descriptors to vectors that account for > 95% variance in data, followed by decision tree classification of the principal components. By utilizing this approach, we observed that the organization of EZH2, RUNX2, Lamin A, SC-35 and H3K4me3 was influenced during differentiation to

differing degrees (Fig. 2C). Interestingly, the organizational metrics of SC-35 were most sensitive to differentiation and led to maximum parsing between basal, adipogenic, and osteogenic treated cells (Fig. 2C and D). The decision tree classification of principal components defining SC-35 organization resulted in > 95% correct classification between cells exposed to basal, adipogenic, and osteogenic media. The predictive model generated had a precision and sensitivity (recall) of 96% and 95%, respectively (Fig 2D, E).

The principal components computed in the analysis and the decision tree classifiers for the various nuclear proteins are included in Fig. S2-S6. Based on these findings, we selected SC-35 as a robust discriminant of stem cell lineages and further explored its organizational behavior as a function of osteogenic factors and microenvironmental cues.

### High content analysis of SC-35 domain descriptors discern dexamethasone-induced bone predisposition within 3 days

Next, we investigated the effect of increasing concentrations of dexamethasone (*dex*), an osteogenic growth factor<sup>32</sup>, on alkaline phosphatase (ALP) expression and SC-35 organization. Levels of 14-day osteogenic differentiation following increased concentrations of *dex* were measured by normalizing number of cells expressing ALP to total cell count (Fig. 3A). As expected, at 14 days there was a positive correlation between increasing *dex* levels in the media and percentage of ALP positive cells in the cell subpopulations. However, at 3 days, confocal images of immunolabeled SC-35 domains of cells exposed to varying concentrations of *dex* showed no observable differences in organization (Fig. 3B). Quantification of individual morphometric features for cell nucleus (i.e., average intensity, nuclear roundness) yielded no observable trends at 3 days as well (Fig. 3C), confirming that conventional imaging tools failed to parse these lineage variations.

Next, using the high content imaging-based algorithm, 26 nuclear texture features defining SC-35 organization were acquired for cells cultured in  $\alpha$ -MEM, and low, medium, and high *dex*, and dimensionally reduced using PCA. A clear separation was observed between the four subpopulations of cells in the PCA plot (Fig. 3D). The PCA plot showed that each of the subpopulations centralized in respective single clusters, indicating that SC-35 texture-based features were highly conserved within the same treatment condition. The predictive decision tree model was further able to correctly classify the cells with a precision of 94% and sensitivity of 93% (Fig. 3E). The decision tree classifier and complete principal component vectors are shown in Fig. S7.

### High content analysis of SC-35 domain descriptors discern surface topography-induced osteogenic fates within 3 days

hMSCs were cultured on films prepared using different ratios of poly(desaminotyrosyl-tyrosine ethyl ester carbonate) (PDTEC) to polystyrene (PS), thus achieving three distinct surface topographies: flat, continuous, and discontinuous (PDTEC islands and glass pits) (Fig. 4A). Culturing hMSCs in osteogenic induction media for 14 days on these topographies

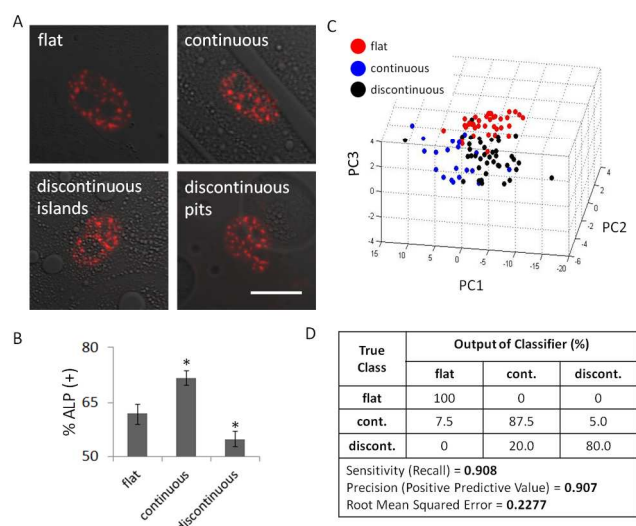


**Fig. 4: SC-35 domain descriptors distinguish surface topography-induced alkaline phosphatase expression within 3 days.** hMSCs were cultured on three distinct surface topographies: flat, continuous, or discontinuous (PDTEC islands and glass pits) for either 3 or 14 days. **(A)** 3 day representative images of SC-35 domains of hMSCs cultured in different surface topographies show no observable differences between the conditions. However, hMSCs cultured for 14 days under the same condition **(B)** show significant differences in percentage of alkaline phosphatase positive cells. hMSCs cultured in the continuous surfaces are significantly more fast blue positive than the control condition (flat), and the discontinuous surfaces feature hMSCs that have significantly less fast blue positive cells than the control condition. For % ALP determination at least 300 cells were counted for each condition. **(C)** PCA plot of 3 day SC-35 domain descriptors show that flat, continuous, and discontinuous can be parsed with a good degree of separation. **(D)** This is independently verified using decision tree analysis. Scale bar = 10  $\mu\text{m}$ . \* indicates statistical significance ( $p < 0.01$ ). For descriptor analysis, between 38 and 44 cells were analysed for each condition.

resulted in significant differences in the percentage of ALP positive cells (**Fig. 4B**). hMSCs cultured on continuous surfaces yielded the highest percentage of ALP positive cells ( $72\% \pm 2\%$ ) whereas cells cultured on discontinuous surfaces had far less osteogenic cells ( $52\% \pm 4\%$ ) when compared to the control flat surface ( $63\% \pm 2\%$ ). These findings confirm that the substrate topography patterns sensitively modulate osteogenic differentiation.

To predict these downstream effects, we sought to investigate how SC-35 organization is affected by the engineered substrates after 3 days in culture. Representative SC-35 images for each condition show that there are no observable differences in SC-35 domains at 3 days for hMSCs cultured on the different surface topographies (**Fig. 4A**). However, high content analysis of SC-35 organization illustrated that cell populations cultured on continuous, discontinuous, and flat surfaces were separated in the 3-D principal component space (**Fig. 4C**). Decision tree analysis generated a predictive classification model that was able to differentiate between cells cultured on the three different topographies with 91% precision and correctly classified instances (**Fig. 4D**). The associated principal component vectors and the decision tree classifier generated are included in **Fig. S8**.

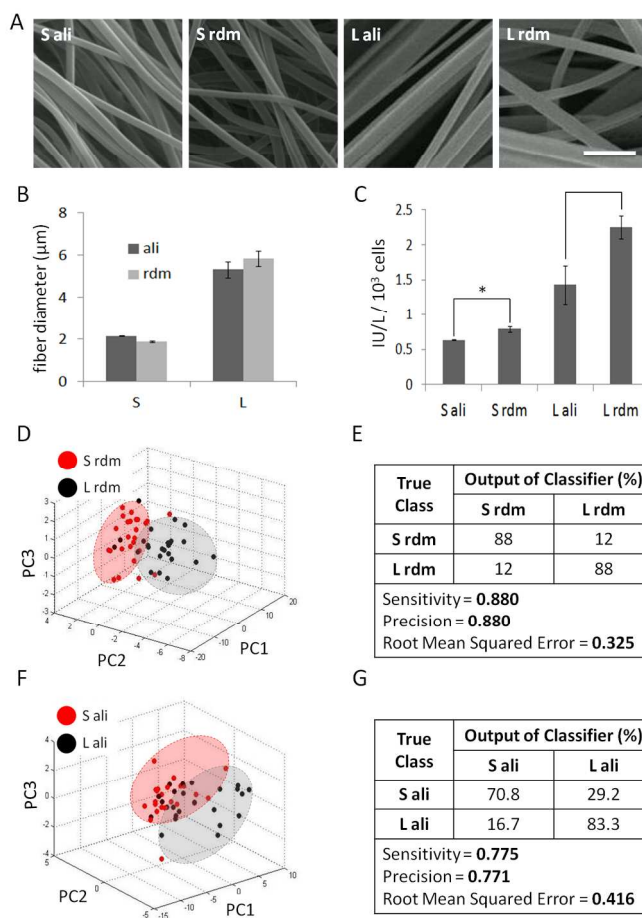


**Fig. 5: SC-35 domain descriptors discern fibrous scaffold topography-induced alkaline phosphatase expression within 3 days.** hMSCs were cultured in BA media on **(A)** fibrous scaffolds featuring fibers of two different sizes and orientations. SEM micrographs of electrospun fibrous scaffolds of two sizes (small, large) and fiber orientations (aligned, random) were used to **(B)** quantify fiber diameters and show that fiber orientation does not significantly affect fiber diameter. Small fibers are distinctly smaller ( $\sim 2 \mu\text{m}$ ) than the large fibers ( $\sim 5.5 \mu\text{m}$ ). **(C)** hMSCs cultured on these fibrous scaffolds for 14 days show distinct alkaline phosphatase activity profiles. For ALP activity determination supernatants from 3 wells measured and averaged for each condition. High content analysis of SC-35 descriptors at 3 days show that hMSCs cultured on **(D-E)** small versus large randomly-oriented fibers and **(F-G)** small versus large aligned fibers can be identified, as confirmed by distinct clusters in PCA plots **(D-F)** and decision tree classification analysis **(E-G)** of PCA-derived principal components. Scale bar = 10  $\mu\text{m}$ . \* indicates statistical significance ( $p < 0.01$ ). For descriptor analysis, at least 20 cells were analysed for each condition.

### Principal component analysis of 3-day SC-35 domain descriptors distinguish bone predisposition outcomes in response to varying fibrous scaffold features

To further highlight the utility of our approach to predict osteogenic differentiation on diverse materials, hMSCs were cultured on fibrous scaffolds featuring fibers of two different sizes (small, large) and orientations (aligned, random) (**Fig. 5A**). Electrospinning settings were optimized so that the fiber diameters were similar ( $\sim 2 \mu\text{m}$  for small,  $\sim 5.5 \mu\text{m}$  for large) for both randomly-oriented and aligned fibers (**Fig. 5B**). hMSCs were cultured in BA media for 14 days and osteogenic differentiation was assessed by measuring ALP activity

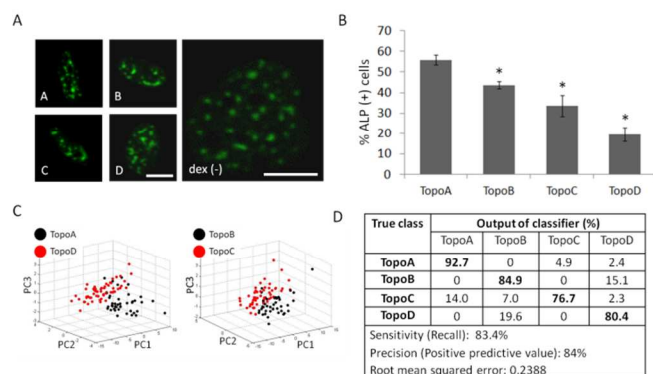


**Fig. 6: SC-35 domain descriptors can identify alkaline phosphatase expression on micropillars within 3 days.** hMSCs were cultured on a subset of micropillars (termed TopoA - TopoD) derived from a much larger library of topographies. (A) Cells show no substantial qualitative differences in SC-35 organization after 3 days in culture, although at 14 days (B) hMSCs cultured in the same conditions displayed significant differences in percentage of alkaline phosphatase positive cells. 3 day SC-35 domain descriptors are capable of identifying differences between the topography culture conditions, as seen by (C) PCA plots of demarcating distinct groupings between the conditions with largest difference in ALP positive cells (TopoA versus TopoD), as well as intermediate ALP positive conditions (TopoB versus TopoC), and (D) decision tree classification analysis of PCA-derived principal components. For analyzing SC-35 organization, between 41 and 56 cells were analysed for each condition. Scale bar = 10  $\mu$ m. \* indicates statistical significance ( $p < 0.01$ ) with respect to TopoA (most osteogenic) condition.

normalized to cell count (Fig. 5C). ALP activity was significantly lower ( $p < 0.01$ ) for hMSCs cultured on the small fibers versus large fibers, irrespective of orientation, while the cells cultured on randomly-oriented, larger fibers had the highest ALP activity.

As illustrated in the PCA plots, our results show that using high content analysis of SC-35 domains at 3 days, cells cultured on small versus large random oriented or aligned fibers could be parsed (Fig. 5D, F). The predictive classification models made using J48 decision tree analysis to classify cells cultured on small versus large fibers had a precision (positive predictive value) and recall of 88% for random fibers, and  $> 77\%$  for aligned fibers (Fig. 5E, G). Complete principal component vectors and the decision tree classifier are included in Fig. S9, S10.

#### Analysis of SC-35 domain descriptors can track hMSC differentiation on micropillars within 3 days

hMSCs were cultured on micropillars featuring distinct topographies prepared using fabrication methods reported by Unadkat et al. in 2010<sup>12</sup>. From a large array of topographical feature combinations, four micropillar patterns with varied features (termed TopoA-D) were selected to further analyze the SC-35 organizational differences in cultured hMSCs. These distinct topographies were observed to be osteoinductive and induced osteogenic differentiation to varied extents. Culturing hMSCs for 14 days in basal media on these topographies resulted in significant differences in percentage of ALP positive cells (Fig. 6B). hMSCs cultured on TopoA had the highest percentage of ALP positive cells ( $56\% \pm 5\%$ ), and a statistically significant ( $p < 0.01$ ) decreasing trend was observed with

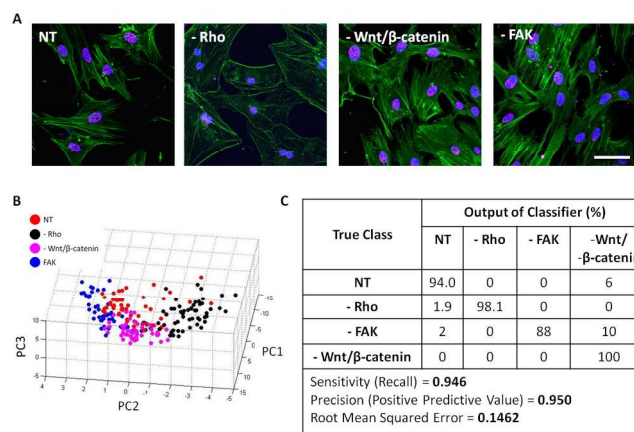


**Fig. 7: Classification for hMSCs treated with different inhibitors using SC-35 organization.** Rho was specifically inhibited using 0.5  $\mu$ g/ml C3 transferase (-RhoGTPase), FAK was inhibited using 1  $\mu$ M FAK inhibitor 14 (-FAK) and Wnt/ $\beta$ -catenin were both inhibited using 15  $\mu$ M FH535. (A) 3 days post culturing cells in presence of inhibitors and OS media, changes in cell morphology were visualized through staining for actin using Alexa488 conjugated phalloidin, for DNA using Hoechst dye and for SC-35 organization using an anti-SC-35 primary and Alexa647 secondary antibody. (B) Subsequently, high content analysis was performed for SC-35 organization and 26 Haralick texture descriptors were evaluated. The descriptors were dimensionally reduced by PCA to principal components that account for 95% of the variance and the principal components were plotted to visualize the cell distribution. (C) Cells treated with different inhibitors were classified using J48 decision tree analysis and the output of the classifier has been presented. At least 50-52 cells were analysed for each condition. Scale bar = 10  $\mu$ m.

TopoB ( $44\% \pm 3\%$ ), TopoC ( $34\% \pm 1\%$ ), and TopoD ( $20\% \pm 3\%$ ). hMSCs cultured on flat surfaces in basal media were used as a negative control and had 0% ALP positive cells, while cells cultured in presence of 1  $\mu$ M *dex* had  $78\% \pm 2\%$  ALP positive cells (data not shown).

To track hMSC phenotypic changes at early time-points, we sought to investigate the influence of micropillar topography on SC-35 organization 3 days post cell culture using high content textural analysis. Representative confocal images for each condition show that there are no observable differences in SC-35 domains at 3 days for hMSCs cultured on the different micropillars (Fig. 6A). On the other hand, as illustrated in the PCA plot, cell populations cultured on the most osteogenic (TopoA) versus the least osteogenic (TopoD) micropillars could be parsed from each other, as well as the two intermediary conditions (TopoB versus TopoC) (Fig. 6C) using high content analysis of SC-35 organization. Decision tree analysis generated a predictive classification model that was able to differentiate between cells cultured on four different micropillar topographies with 83% sensitivity and 84% precision (Fig. 6D). Interestingly, cells cultured in the two conditions that induced the least ALP (Topo C and TopoD) showed the most distinct changes in SC-35 organization. 14% of cells cultured in TopoC were incorrectly classified as belonging to TopoA, which elicited a significantly higher percentage of ALP positive hMSCs. Similarly, classification of cells cultured in TopoD, the least ALP-inducing condition, binned 80% correctly and classified 20% of the cells as belonging to TopoB, which induced a significantly higher

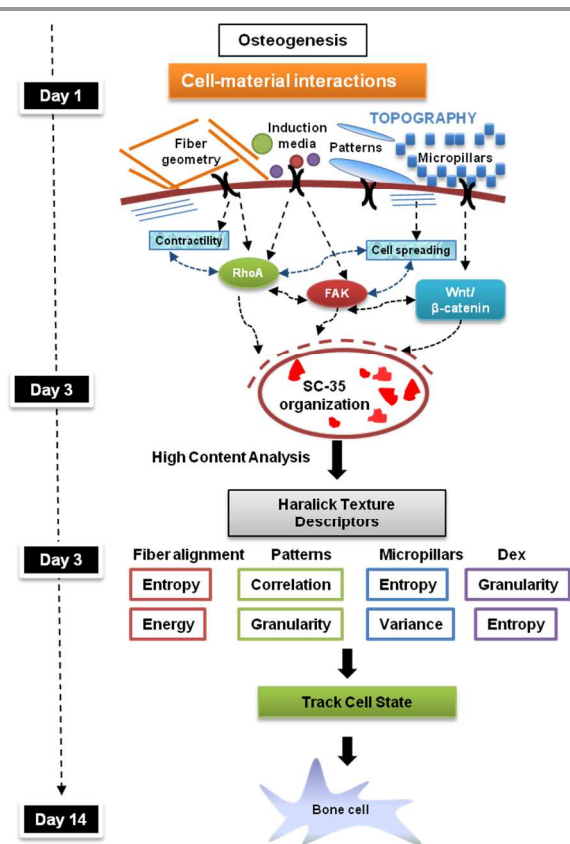


**Fig. 8: Tracking microenvironment modulated osteogenic differentiation using SC-35.** Cell-material interactions induce osteogenic differentiation by modulating actin dynamics and signaling cascades mediated by RhoA, Fak, and Wnt/ $\beta$ -catenin signaling. These signaling cascades direct changes in the transcriptional machinery that regulate the gene expression and cell phenotype. Our study indicates that SC-35 organizational dynamics are sensitive to these changes and can be used to track osteogenic lineage commitment at early time-points in response to cell-material interactions.

percentage of ALP positive hMSCs (Fig. 6D). Complete principal component vectors are described in Fig. S11.

### Pharmacological inhibition of signaling molecules governing osteogenesis results in quantifiable alterations in SC-35 organization

To elucidate the cross-talk between adhesion signaling and SC35 organization, the roles of several molecules, namely, RhoGTPase, FAK1, and  $\beta$ -catenin on SC-35 organization were investigated. RhoGTPase, FAK1, and  $\beta$ -catenin were specifically inhibited using 0.5  $\mu$ g/ml C3 transferase (C3), 1  $\mu$ M FAK inhibitor, and 15  $\mu$ M FH353, respectively. At the mentioned inhibitor concentrations, the cell viability was not significantly affected at time of SC-35 organization analysis which was performed 3 days post culturing cells in osteogenic induction media (Fig. S13A). hMSCs were cultured in OS induction media in the presence of inhibitors for 14 days and osteogenic differentiation was assessed by staining for ALP. As expected, treatment with pharmacological inhibitors resulted in almost no ALP positive cells at 14 days (Fig. S13B). At 3 days, RhoGTPase inhibition drastically reduced polymerized actin fibers in the cells, whereas treatment with FAK and  $\beta$ -catenin

did not significantly influence actin polymerization or cell morphology (Fig. 7A). Interestingly, PCA plot of 3 day assessment of the SC-35 organization showed good separation between the different inhibition treatment groups (Fig. 7B). This is supported by decision tree analysis, which shows almost 95% of cells are correctly classified (Fig. 7C). Complete principal component vectors and the decision tree classifier generated are shown in Fig. S14.

### Tracking microenvironment-mediated osteogenic differentiation using Haralick texture features of SC-35 domains

On the basis of our findings, we propose a model for tracking microenvironment modulated osteogenic differentiation using SC-35 as a surrogate marker (Fig. 8). According to this model, microenvironmental cues investigated in this manuscript including soluble growth factors, fibrous scaffolds, patterned substrates, and micropillars steer hMSCs towards osteogenic differentiation by 14 days by influencing early cytoskeletal dynamics and intracellular signaling pathways mediated by Rho, FAK, and Wnt/ $\beta$ -catenin. These signaling cascades induce changes in the transcriptional machinery, thereby modulating the gene expression and SC-35 organizational dynamics. Our model proposes that the effect of microenvironmental cues on stem cell phenotype be tracked using SC-35 organizational metrics at 3 days (Fig. 8).

The descriptors used to quantify the organization of SC-35 can be sub-classified into four groupings: entropy, correlation, granularity, and inertia, which represent a measure of speckle homogeneity, elongation, size, and distribution with respect to nuclear centroid, respectively. The potential biological relevance for each feature has been listed in Table S1.

The contribution of individual descriptors was evaluated by measuring information gain with respect to each condition, using the Weka machine learning software. The top 10 descriptors were ranked on the basis of information gain and listed for each condition in Tables S2, S3. Our attribute evaluation indicated that granularity and entropy descriptors were the most informational texture descriptors accounting for changes in the SC-35 organization in response to soluble cues. Interestingly, the most informational SC-35 organizational Haralick descriptors were different for hMSCs cultured on the distinct topographical platforms. Correlation, granularity and inertia descriptors had the maximum information gain about SC-35 organizational dynamics in hMSCs cultured on surface topographies featuring different degrees of continuity (patterns), while entropy and variance descriptors were most relevant about SC-35 dynamics in hMSCs cultured on varied micropillars. In contrast, on fibrous scaffolds, entropy descriptors provided maximum information gain about SC-35 organizational changes (Table S3).

These findings show that interactions of hMSCs with different microenvironmental cues lead to specific and distinct emergent patterns of SC-35 descriptors that govern the divergent osteogenic differentiation traits as early as 3 days.

The relevance of textural attributes in defining SC-35 organizational metrics modulated by different signaling molecules (RhoGTPase, FAK, Wnt/ $\beta$ -catenin) was also evaluated (Tables S4). Entropy and correlation descriptors had the maximum information gain about SC-35 organizational dynamics in response to RhoGTPase and Wnt/ $\beta$ -catenin inhibition in hMSCs, while entropy and inertia descriptors were most relevant about SC-35 dynamics in hMSCs exposed to FAK inhibition. This indicates that the different signaling molecules involved in modulating osteogenic differentiation in response to various matrix constraints differentially influence SC-35 organizational metrics. Therefore, as indicated in the proposed model, the differential spatial localization of SC35 under various matrix constraints is possibly a consequence of a complex cascade of intracellular signalling events and distinct cell states.

## Discussion

In this study, we have developed and demonstrated the applicability of an integrated framework based on high content image informatics to develop predictive classification models that can discern and classify changes in cell state in response to cell-microenvironment interactions.

First, different nuclear proteins (i.e., SC-35, EZH2, RUNX2, Lamin A, and H3K4me3) were screened to determine how their nuclear organization was influenced at early time-points upon initiation of growth factor-induced differentiation. Our results showed that SC-35 organization was maximally influenced early on (3 days) during the differentiation process. By employing the algorithm presented in this paper, SC-35 organization could be used to generate a predictive model to classify cells exposed to basal, osteogenic, and adipogenic induction media with a positive predictive value of 96%. Further, using SC-35 organization metrics hMSCs exposed to different concentrations of soluble cues, specifically dexamethasone (*dex*), an osteogenic differentiation factor, could be parsed with > 90% precision and sensitivity. These findings show that SC-35 domains are highly sensitive to activation via growth factors that steer hMSCs towards distinct lineages. Several accounts of literature suggest that spliceosomes within the SC-35 domains aggregate at the active transcription sites of genes regulating the differentiation of several lineages including myogenesis<sup>33</sup>, adipogenesis<sup>34</sup>, and osteogenesis<sup>35</sup>. When transcription is halted via the use of pharmacological inhibitors, splicing factors aggregate into large, round speckles<sup>36</sup>. In contrast, when transcription is high, the accumulation of splicing factors is reduced, and they redistribute to nucleoplasmic transcription sites<sup>37</sup>. Another notable property of SC-35 domains is that the domains reside in interchromatin regions<sup>38</sup>, which contain little or no DNA<sup>39</sup>. Consequentially, the organization of SC-35 domains may serve as an indirect measure of global chromatin changes regulated by outside-in signaling which links focal adhesions, actin, and the nuclear space<sup>40</sup>.

Biomaterial topography effectively regulates stem cell differentiation by modulating cell-shape<sup>4</sup>. Thus, we sought to elucidate the degree to which SC-35 organization was sensitive to three variable osteogenic microtopographies: surface patterns, fibrous scaffolds, and micropillars. Surface-induced phase separation can be utilized to produce well-defined, easily replicated, and well-characterized surfaces presenting a wide range of topographical features<sup>41</sup>. Here, this fabrication method was adapted to construct surfaces with three distinct patterns: flat, continuous ridges, and discontinuous islands and pits. Our results indicate that osteogenic differentiation is enhanced in hMSCs sensing continuous surfaces. This correlates with previous studies where osteogenic differentiation mediated by Wnt/ $\beta$ -catenin signaling has been shown to be regulated on grooved surfaces<sup>42</sup>. Furthermore, using SC-35 organization nuclear metrics, the influence of surface topography on osteogenic differentiation could be predicted with > 90% precision and sensitivity.

Next, we applied our high content imaging methodology to predict the differentiation potential of hMSCs cultured within microfibrous scaffolds prepared by electrospinning<sup>43-45</sup>. Electrospun fibrous scaffolds were chosen since they have wide applicability for bone tissue engineering applications<sup>46-48</sup>. Fibers with a larger diameter of 5  $\mu$ m induced significant osteogenic differentiation in hMSCs ( $p < 0.01$ ) as compared to fibers with a smaller diameter of 2  $\mu$ m, indicating that the variations in the chosen fiber scaffold geometries modulate osteogenic differentiation. These results are consistent with electrospun fiber geometries reported to regulate osteogenic differentiation<sup>49</sup>. By exposing hMSCs to various growth factors and topographies, we have demonstrated that the onset of osteogenic differentiation on a diverse set of culture conditions can be predicted by mapping early SC-35 organizational features.

There has also been an increased interest in characterizing the role of bulk substrate properties on the differentiation of stem cell populations. In the context of bone, biomaterials with high elastic modulus featuring different topographical patterns have been investigated<sup>50</sup>. Previously, an algorithm-based approach was developed to produce chips featuring over 2,000 micropillars in efforts to identify topographies that maximize mitogenic and osteogenic responses<sup>12</sup>. This study identified "hit" surfaces that corresponded to high alkaline phosphatase expression without the presence of osteogenic growth factors, but the methods presented relied on a population-based readout at a late time-point (10 days) that may not account for potential heterogeneous responses within a particular topographical condition.

As such, we applied our methodology to classify hMSCs cultured on a subset of micropillars chosen from a library of 2,176 distinct, randomly designed surface topographies using methods previously published<sup>12</sup>. We chose topographies based on their ability to induce varying percentages of ALP positive without the presence of *dex* after 14 days in culture. Using our high content analysis, we correctly identified individual cells as belonging to either of four micropillars. Using the classification

algorithm based on SC-35 organization, we could predict topography-induced ALP expression as well as quantitatively identify differences in cell state within a culture condition, for example, cells cultured in TopoD, the least ALP-inducing condition, were parsed 80% correctly as cells on TopoD and 20% as cells on TopoB, which induced a significantly higher percentage of ALP positive hMSCs. This is of particular interest when performing studies with cell lines that are innately heterogeneous.

Microenvironmental cues, specifically soluble factors, topography, and substrate surface functionality, have been shown modulate hMSC differentiation through  $\beta$ -catenin<sup>42, 51</sup>, FAK<sup>52, 53</sup>, and RhoGTPase<sup>54</sup>, which are key signaling molecules that direct osteogenic differentiation<sup>18, 55, 56</sup>. Surface topography modulates Wnt/ $\beta$ -catenin signaling through primary cilia structure<sup>42</sup>, and increased Wnt/ $\beta$ -catenin is observed in hMSCs cultured on rough topographies<sup>57</sup>. Recently, FAK has been implicated in the modulation of hMSC differentiation by microenvironmental cues such as substrate surface functionalities<sup>52</sup> and microtopographies<sup>53</sup>, where RhoGTPase has been shown to regulate osteogenesis through fiber geometries<sup>54</sup>. FAK and RhoA have also been shown to positively regulate osteogenesis<sup>58</sup> and negatively regulate adipogenesis of hMSCs using induction media<sup>59</sup>.

An initial microarray analysis of hMSCs cultured in osteoinductive media for 24 hours showed a significant increase ( $p < 0.05$ ) in RhoA and FAK gene expression as compared to cells cultured in basal media, which correlated with a significant up-regulation ( $p < 0.05$ ) of SC-35 gene expression (Fig. S12). On the other hand, for cells cultured in adipogenic media microarray analysis indicated a significant increase in  $\beta$ -catenin and a significant decrease in SC-35 gene expression as compared to cells cultured in basal media (Fig. S12). To obtain a more comprehensive understanding of how SC-35 organization is regulated during osteogenic differentiation, we investigated the influence of  $\beta$ -catenin, FAK, and RhoGTPase-mediated signaling on SC-35 domains. Using our algorithm, SC-35 organization was highly sensitive to specific inhibition of these molecules. Changes in cell state on inhibition of  $\beta$ -catenin, FAK, and RhoGTPase could be detected and classified with  $> 95\%$  precision using high content analysis of SC-35 organization. This suggests a possible mechanism for how SC-35 organization is responsive to osteogenic differentiation via osteogenic signaling molecules.

Furthermore, our results show that the influence of different matrix constraints (topography, fiber diameter) on SC-35 organizational metrics is manifested through distinct changes in textural attributes. For example, during early phases of osteogenic differentiation, the micropillar topography alters SC-35 organization by modifying the entropy and variance textural descriptors, while surface topographies featuring different degrees of continuity (patterns) modify the correlation and inertia descriptors. Based on our findings we propose a model (Fig 8) wherein different microenvironmental cues lead to complex and distinct signaling cascades that modulate

osteogenic differentiation, leading to emergent cell states represented by unique SC-35 organizational signatures.

In summary, our results indicate that microenvironmental cues affect key signaling molecules, which modulate both the early organization of SC-35 (3 day), as well as long-term stem cell lineage commitment (14 day). Using high content image acquisition we can identify and profile these early, single-cell sc-35 organizational changes indicative of stem cell differentiation. This is important, because single cell analyses have the potential to address current limitations in current population-based assays, which are unable to account for population heterogeneity and require stem cells to be fully differentiated.

## Materials and Methods

### Cell Culture

Human mesenchymal stem cells (hMSCs) were obtained from Texas A&M University (College Station, TX). Cells were cultured in a humidity-controlled environment under 5% CO<sub>2</sub> and 37°C and fed every 3 to 4 days with basal growth media (BA) supplemented with fetal bovine serum (FBS) (10% v/v) and penicillin-streptomycin (0.1% v/v). Cells were received at passage 1 and used for up to 5 passages. hMSCs were expanded in BA media and upon reaching 60% confluence trypsinized and plated according to experiment-dependent conditions. Osteogenic differentiation (OS) was induced by culturing hMSCs in BA media supplemented with L-ascorbic acid-2-phosphate, dexamethasone (*dex*), and  $\beta$ -glycerophosphate<sup>2</sup>. Adipogenic differentiation (AD) was induced with BA media supplemented with *dex*, indomethacin, insulin, and 3-isobutyl-1-methyl-xanthine for induction, and adipogenic maintenance media was composed of BA media supplemented with insulin. Adipogenic media in AD conditions was cycled with 3 days induction followed by 1 day maintenance. hMSCs were plated at optimal differentiation-inducing densities of 10,000 cells/cm<sup>2</sup>, 21,000 cells/cm<sup>2</sup>, and 5,000 cells/cm<sup>2</sup> for BA, AD, and OS conditions, respectively. Unless otherwise stated, cells were allowed to adhere for 6 hours in basal growth media, followed by a media change with appropriate induction media.

### Fabrication of Surface Textures

Surface patterns were fabricated using phase separation of two immiscible polymers via demixing using principles previously reported<sup>41</sup>. Varying ratios of poly(desaminotyrosyl-tyrosine ethyl ester carbonate) (PDTEC) and polystyrene (PS) were dissolved in tetrahydrofuran (THF) to create a 2% (w/v) polymer solution<sup>60</sup>. Polymer solutions were spin-coated onto 12 mm glass coverslips at 4000 RPM for 30 seconds, resulting in a thin film of phase-separated PDTEC and PS. Six different surface pattern topographies were created by varying the PDTEC:PS ratio (100:0, 80:20, 60:40, 40:60, 20:80, 0:100). Cyclohexane was used to remove PS, resulting in PDTEC polymeric surface patterns varying in degree of PDTEC polymer continuity. Coverslips were vacuum dried overnight to

remove residual cyclohexane. Lastly, prior to culturing hMSCs, films were stored in a desiccator, sterilized with UV light for 900 seconds, and washed three times with phosphate buffered saline (PBS) (Lonza).

### Fabrication and Characterization of Microfibrous Scaffolds

Fibrous scaffolds were fabricated using an electrospinning apparatus. Low viscosity solutions of PDTEC were prepared in a volatile solvent as tabulated below. The needle of the syringe containing the solvent was maintained at a positive charge (+keV) and placed 6 cm from the collecting rotating mandrel that was maintained at a negative charge (-keV). The flow rate of the polymer solution was controlled by a syringe pump. The micrometer-sized fibers were deposited on the mandrel as the solvent evaporated from the solution streaming out of the syringe. The alignment of these fibers was controlled by the speed of the mandrel; higher speeds resulting in higher orientation. The diameter of the fibers was controlled by the viscosity of the polymer solution by changing the polymer concentration (from 14% to 18% w/v). Higher viscosity resulted in larger diameter fibers in the scaffold<sup>61</sup>. Polymer solution compositions and the electrospinning conditions are summarized in **Table 1**.

Size	Polymer	Solvent	wt/v%	flow rate	
				+keV	-keV
S	PDTEC	HFIP	14	3 mL/hr	18 -6
L	PDTEC	MeCl <sub>2</sub>	18	3 mL/hr	24 -6

**Table 1:** Summary of electrospinning parameters for fibrous scaffolds.

### Fabrication of Micropillars

Topographies were designed and fabricated using previously published methods<sup>12</sup>. Briefly, micropillar patterns were generated by utilizing an algorithm that randomly selected parameters for: (1) size of pattern, (2) number and distribution of primitive shapes (i.e., triangles, circles, and rectangles), and (3) size and degree of alignment of primitives. The micropillar designs were then etched to a silicon wafer which was used to generate a silicon master. Hot embossing of polystyrene films (250 μm thick) was then performed by sandwiching between the silicon master and an Obducat UV Sheet Polyester (100 Micron 10638). Imprinting was carried out at 80°C at a pressure of 30 bars for 10 minutes. After cooling, assembly was demoulded and micropillars were detached using a wafer saw.

### Fluorescence- and Immuno-staining for Confocal Imaging

hMSCs were fixed with 4% paraformaldehyde (Electron Microscopy Sciences) for 15 minutes. Next, samples were blocked and permeabilized with a 0.1% Triton X-100 (Sigma) / 5% normal goat serum (MP Biomedicals) solution in PBS. After two washes with blocking buffer (5% NGS in PBS), primary antibodies specific to proteins of interest were added at different concentrations overnight at 4°C, as indicated in the **Table 2**.

Reporter	Description	Catalog#
SC-35	Mouse monoclonal [SC-35] to SC35 (phospho) - Nuclear Speckle Marker	ab11826
EZH2	Rabbit polyclonal to KMT6 / EZH2 - ChIP Grade	ab3748
RUNX2	Mouse monoclonal to RUNX2	ab54868
Lamin A	Mouse monoclonal [133A2] to LaminA	ab8980
H3K4me3	Rabbit polyclonal to Histone H3 (tri methyl K4) - ChIP Grade	ab8580

**Table 2: List of primary antibodies used in the study.** All primary antibodies were obtained from Abcam. The SC35 antibody was diluted 1:500 for usage while the others were used at 1:200 dilution factor.

After three 15 minute washes in blocking buffer, secondary antibodies (Alexa Fluor; Invitrogen) with different fluorophores and corresponding isotype controls in blocking buffer at a 1:250 ratio were added for 2 hours at room temperature. To label the actin cytoskeleton, cells were fixed and stained with Alexa Fluor 488 phalloidin (Invitrogen) per the manufacturer's instructions. All samples were counterstained with 5 μg/ml Hoescht (Sigma) in PBS and stored at 4°C until imaging. To acquire high resolution images, samples were imaged under a 63x objective with a Leica TCS SP2 system (Leica Microsystems).

### Analysis of Nuclear Protein Organization

To analyze the organization of nuclear proteins, 26 texture-based Haralick texture features were acquired for each cell. First, images underwent intensity-based thresholding to create nuclear ROI masks for each nucleus in a given image, based on Hoescht DNA staining. Next, Haralick descriptors were obtained using a Matlab algorithm. A complete list of the calculated Haralick descriptors with their definitions is provided in **Table S1**. These descriptors are quantifiable measurements of texture features that represent the spatial organization of the nuclear proteins. Weka (Waikato Environment for Knowledge Analysis) is an open-source machine learning software that was developed at University of Waikato, New Zealand. The 26 descriptors were linearly reduced to a minimum number of eigenvectors that account for 95% variance of the data by performing principal component analysis (PCA) using the Weka open source software. PCA transformed data was exported and plotted in Matlab (MathWorks, Natick, MA) to obtain a PCA plot where each point represents a stem cell in 3-D space, and where each axis represents a computed principal component. Therefore, each point is represented by a unique set (x, y, z) of principal components (eigenvectors).

To illustrate differences between the various subpopulations, a predictive classification model was made using J48 decision tree analysis in the Weka software. J48 generated a C4.5 pruned decision tree, where tree pruning is used as a tool to correct for potential over fitting. The best performing classification tree was generated by using the experimental data as the training set. The quality of the tree is reported in terms of the percent of correctly classified instances, precision (positive predictive value), and recall (sensitivity).

Briefly, Precision = TP/(TP+FP) and Recall = TP/ (TP+FN). True positives (TP) are the number of instances correctly classified as belonging to the positive class. False positives (FP) are the number of instances incorrectly classified to the class. False negatives (FN) are the number of instances not classified to the class but belong to class. Precision is also defined as the number of instances that truly have class x among all those which are classified as class x.

### Assessment of Cell Differentiation

To quantify differentiation, hMSCs cultured in induction media were either fixed or lysed at 14 days. Fixed cells were stained for alkaline phosphatase (ALP) (fast blue RR, Sigma) or intracellular triglycerides (AdipoRed, Lonza) per the manufacturer's instructions. Samples were then counterstained with Hoescht to identify osteogenic- and adipogenic-positive cells. Lysed samples were either used to determine ALP concentrations using an ALP activity assay per manufacturer's instructions (QuantiChrom™), or the relative gene expression of ALP (Qiagen, ALP)<sup>62</sup> or lipoprotein lipase (Qiagen, LPL), as previously reported<sup>62</sup>.

### Inhibition of RhoGTPase, FAK, and Wnt/β-catenin

Rho was specifically inhibited using cell permeable C3 transferase (C3, Cytoskeleton, Denver, CO) and FAK was inhibited using FAK inhibitor 14 (SantaCruz Biotechnology, Dallas, Texas). Wnt/β-catenin was inhibited using cell-permeable FH535<sup>63, 64</sup> (SantaCruz Biotechnology, Dallas, Texas). hMSCs were seeded in a 8-well Labtek at a cell density of 8,000 cells per well and allowed to attach overnight (12 hours) in basal media, before media in the wells was replaced with serum-free media containing 0.5 μg/ml C3 transferase (C3) for 4 hours, or 1 μM FAK inhibitor 14 for 1 hour, or 15 μM FH535 for 1 hour. After pre-treatment, media was changed with induction media containing the inhibitor. Adipogenic media in AD conditions was cycled with 3 days induction followed by 1-day maintenance. Basal and osteogenic media was cycled every three days. Cell proliferation was analyzed 3 days post induction (time of descriptor analysis) using Alamar Blue assay using manufacturer's protocol.

### Statistics

Statistical analysis of morphometric parameters included analysis of variance (ANOVA) with Tukey's honestly significant difference (HSD) post hoc method and other multivariate statistical tools. The differences were considered significant for  $p < 0.05$  unless otherwise noted. Error bars indicate the standard uncertainty around the mean.

### Conclusions

In conclusion, we have advanced a methodology based on high content imaging of SC-35 organization in the nucleoplasm, in concert with machine learning approaches, for predictive modeling of hMSC differentiation mediated by

microenvironmental cues such as differentiation media, soluble factors, and substrate topography. The SC-35 parsing approach could successfully detect and classify hMSC differentiated phenotypes on different surface topographies and microfiber geometries (fibrous scaffolds and micropillars). Further, SC-35 organization can capture changes in cell state modulated by signaling molecules involved in osteogenic differentiation, specifically RhoGTPase, FAK1, and Wnt/β-catenin. Such a predictive model may elucidate the emergent lineage restriction in more complex microenvironments and also provide in silico informatics of stem cell lineages on biomaterials that steer stem cells toward strategic, regenerative phenotypes.

### Acknowledgments

This study was supported by funding from NIH EB001046 (RESBIO, Integrated Resources for Polymeric Biomaterials) and NSF DGE 0801620 (IGERT on Integrated Science and Engineering of Stem Cells).

### Notes and references

- <sup>#</sup> These authors contributed equally to the manuscript  
<sup>a</sup> Department of Chemical and Biochemical Engineering, Rutgers University, Piscataway New Jersey.  
<sup>b</sup> Department of Biomedical Engineering, Rutgers University, Piscataway New Jersey.  
<sup>c</sup> New Jersey Medical School, Rutgers University, Newark New Jersey.  
<sup>d</sup> Department of Tissue Regeneration, MIRA Institute for Biomedical Technology and Technical Medicine, University of Twente, Enschede, The Netherlands.  
<sup>e</sup> cBITE Lab, MerIn Institute for Technology-Inspired Regenerative Medicine, Maastricht University, Maastricht, The Netherlands.  
<sup>f</sup> Department of Chemistry and Chemical Biology, New Jersey Center for Biomaterials, Rutgers University, Piscataway, New Jersey.  
<sup>\*</sup> Corresponding Author: Prabhias Moghe  
 599 Taylor Road, Piscataway, NJ 08854.  
 E-mail: moghe@rutgers.edu, Phone: 848-446-6591  
<sup>†</sup> Electronic supplementary information (ESI) available: Supplementary Figure 1 showing SC-35 expression in hMSCs cultured in different induction media (BA, AD, OS). Supplementary Figure 2 showing hMSC phenotype classification using EZH2 organization for cells exposed to different culture media. Supplementary Figure 3 showing hMSC phenotype classification using RUNX2 organization for cells exposed to different culture media. Supplementary Figure 4 showing hMSC phenotype classification using Lamin A organization for cells exposed to different culture media. Supplementary Figure 5 showing hMSC phenotype classification using H3K4me3 organization for cells exposed to different culture media. Supplementary Figure 6 showing hMSC phenotype classification using SC-35 organization for cells exposed to different culture media. Supplementary Figure 7 showing classification of hMSCs cultured in presence of different dexamethasone (*dex*) concentrations using SC-35 organization. Supplementary Figure 8 showing cell state classification for hMSCs cultured on patterned surfaces using SC-35 organization. Supplementary Figure 9 showing cell state classification for hMSCs cultured on randomly-oriented fibers using SC-35 organization. Supplementary Figure 10 showing cell state classification for hMSCs cultured on aligned fibers using SC-35 organization. Supplementary Figure 11 listing principal components for cell state classification for hMSCs cultured on different micropillars using

SC-35 organization. Supplementary Figure 12 showing microarray analysis of RhoA, FAK, and  $\beta$ -catenin expression in hMSCs cultured in BA, AD and OS media. Supplementary Figure 13 showing effects of pharmacological inhibitors on cell viability and osteogenic differentiation. Supplementary Figure 14 showing classification of hMSCs treated with different inhibitors using SC-35 organization. Supplementary Table S1 lists the 13 Haralick texture features used in this study. Supplementary Tables S2, S3 and S4 summarize the most significant Haralick features across diverse culture conditions.

1. A. I. Caplan, *J Orthop Res*, 1991, **9**, 641-650.
2. M. F. Pittenger, A. M. Mackay, S. C. Beck, R. K. Jaiswal, R. Douglas, J. D. Mosca, M. A. Moorman, D. W. Simonetti, S. Craig and D. R. Marshak, *Science*, 1999, **284**, 143-147.
3. J. M. Curran, R. Chen and J. A. Hunt, *Biomaterials*, 2006, **27**, 4783-4793.
4. D. E. Discher, D. J. Mooney and P. W. Zandstra, *Science*, 2009, **324**, 1673-1677.
5. F. Guilak, D. M. Cohen, B. T. Estes, J. M. Gimble, W. Liedtke and C. S. Chen, *Cell Stem Cell*, 2009, **5**, 17-26.
6. D. E. Discher, P. Janmey and Y. L. Wang, *Science*, 2005, **310**, 1139-1143.
7. A. J. Engler, S. Sen, H. L. Sweeney and D. E. Discher, *Cell*, 2006, **126**, 677-689.
8. U. Krause, A. Seckinger and C. A. Gregory, *Methods Mol Biol*, 2011, **698**, 215-230.
9. Z. Yang, J. F. Schmitt and E. H. Lee, *Methods Mol Biol*, 2011, **698**, 353-366.
10. D. G. Anderson, D. Putnam, E. B. Lavik, T. A. Mahmood and R. Langer, *Biomaterials*, 2005, **26**, 4892-4897.
11. A. A. Moe, M. Suryana, G. Marcy, S. K. Lim, S. Ankam, J. Z. Goh, J. Jin, B. K. Teo, J. B. Law, H. Y. Low, E. L. Goh, M. P. Sheetz and E. K. Yim, *Small*, 2012, **8**, 3050-3061.
12. H. V. Unadkat, M. Hulsman, K. Cornelissen, B. J. Papenburg, R. K. Truckenmuller, A. E. Carpenter, M. Wessling, G. F. Post, M. Uetz, M. J. Reinders, D. Stamatialis, C. A. van Blitterswijk and J. de Boer, *Proc Natl Acad Sci U S A*, 2011, **108**, 16565-16570.
13. A. Scuteri, E. Donzelli, D. Foudah, C. Caldara, J. Redondo, G. D'Amico, G. Tredici and M. Miloso, *Int J Stem Cells*, 2014, **7**, 127-134.
14. G. M. de Peppo, H. Agheli, C. Karlsson, K. Ekstrom, H. Brisby, M. Lenneras, S. Gustafsson, P. Sjoval, A. Johansson, E. Olsson, J. Lausmaa, P. Thomsen and S. Petronis, *Int J Nanomedicine*, 2014, **9**, 2499-2515.
15. H. Xing, Y. Taguchi, S. Komasa, I. Yamawaki, T. Sekino, M. Umeda and J. Okazaki, *J Periodontol*, 2014, 1-20.
16. B. Shen, A. Wei, S. Whittaker, L. A. Williams, H. Tao, D. D. Ma and A. D. Diwan, *J Cell Biochem*, 2010, **109**, 406-416.
17. K. A. Kilian, B. Bugarija, B. T. Lahn and M. Mrksich, *Proc Natl Acad Sci U S A*, 2010, **107**, 4872-4877.
18. R. McBeath, D. M. Pirone, C. M. Nelson, K. Bhadriraju and C. S. Chen, *Dev Cell*, 2004, **6**, 483-495.
19. E. Liu, S. Gordonov, M. D. Treiser and P. V. Moghe, *Cell Cycle*, 2010, **9**, 2108-2117.
20. M. D. Treiser, E. H. Yang, S. Gordonov, D. M. Cohen, I. P. Androulakis, J. Kohn, C. S. Chen and P. V. Moghe, *Proceedings of the National Academy of Sciences of the United States of America*, 2010, **107**, 610-615.
21. S. L. Vega, E. Liu, P. J. Patel, A. B. Kulesa, A. L. Carlson, Y. Ma, M. L. Becker and P. V. Moghe, *J Biomol Screen*, 2012, **17**, 1151-1162.
22. J. J. Kim, S. L. Vega and P. V. Moghe, *Methods Mol Biol*, 2013, **1052**, 1-8.
23. J. D. Pajerowski, K. N. Dahl, F. L. Zhong, P. J. Sammak and D. E. Discher, *Proc Natl Acad Sci U S A*, 2007, **104**, 15619-15624.
24. Y. Wei, Y. H. Chen, L. Y. Li, J. Lang, S. P. Yeh, B. Shi, C. C. Yang, J. Y. Yang, C. Y. Lin, C. C. Lai and M. C. Hung, *Nat Cell Biol*, 2011, **13**, 87-94.
25. R. Akter, D. Rivas, G. Geneau, H. Drissi and G. Duque, *J Bone Miner Res*, 2009, **24**, 283-293.
26. J. Swift, I. L. Ivanovska, A. Buxboim, T. Harada, P. C. Dingal, J. Pinter, J. D. Pajerowski, K. R. Spinler, J. W. Shin, M. Tewari, F. Rehfeldt, D. W. Speicher and D. E. Discher, *Science*, 2013, **341**, 1240104.
27. K. S. Lee, H. J. Kim, Q. L. Li, X. Z. Chi, C. Ueta, T. Komori, J. M. Wozney, E. G. Kim, J. Y. Choi, H. M. Ryoo and S. C. Bae, *Mol Cell Biol*, 2000, **20**, 8783-8792.
28. A. Noer, L. C. Lindeman and P. Collas, *Stem Cells Dev*, 2009, **18**, 725-736.
29. X. D. Fu and T. Maniatis, *Nature*, 1990, **343**, 437-441.
30. D. L. Spector and A. I. Lamond, *Cold Spring Harb Perspect Biol*, 2011, **3**.
31. R. M. Haralick, Shanmugam, K., Dinstein, I., *Systems, Man and Cybernetics*, 1973, **SMC-3**, 610-621.
32. N. Jaiswal, S. E. Haynesworth, A. I. Caplan and S. P. Bruder, *Journal of cellular biochemistry*, 1997, **64**, 295-312.
33. P. T. Moen, Jr., C. V. Johnson, M. Byron, L. S. Shopland, I. L. de la Serna, A. N. Imbalzano and J. B. Lawrence, *Mol Biol Cell*, 2004, **15**, 197-206.
34. I. Szczerbal and J. M. Bridger, *Chromosome Res*, 2010, **18**, 887-895.
35. M. Romero-Prado, C. Blazquez, C. Rodriguez-Navas, J. Munoz, I. Guerrero, E. Delgado-Baeza and J. P. Garcia-Ruiz, *J Cell Biochem*, 2006, **98**, 1457-1470.
36. I. Melcak, S. Cermanova, K. Jirsova, K. Koberna, J. Malinsky and I. Raska, *Mol Biol Cell*, 2000, **11**, 497-510.
37. L. F. Jimenez-Garcia and D. L. Spector, *Cell*, 1993, **73**, 47-59.
38. D. L. Spector, X. D. Fu and T. Maniatis, *Embo J*, 1991, **10**, 3467-3481.
39. M. Thiry, *Histol Histopathol*, 1995, **10**, 1035-1045.
40. J. J. Kim, R. I. Cohen, M. S. Devita, N. K. Bennet, S. Chahar, S. Vishwananth, E. A. Lee, G. Jung, P. P. Shao, E. P. Childers, S. Liu, B. A. Garcia, M. L. Becker, N. S. Hwang, A. Madabhushi, M. P. Verzi and P. V. Moghe, *In Preparation*, 2015.
41. M. Boltau, S. Walheim, J. Mlynek, G. Krausch and U. Steiner, *Nature*, 1998, **391**, 877-879.
42. R. J. McMurray, A. K. Wann, C. L. Thompson, J. T. Connelly and M. M. Knight, *Sci Rep*, 2013, **3**, 3545.
43. G. Kumar, C. K. Tison, K. Chatterjee, P. S. Pine, J. H. McDaniel, M. L. Salit, M. F. Young and C. G. Simon, Jr., *Biomaterials*, 2011, **32**, 9188-9196.
44. A. S. Nathan, B. M. Baker, N. L. Nerurkar and R. L. Mauck, *Acta Biomater*, 2011, **7**, 57-66.

## Journal Name

45. E. K. Yim, E. M. Darling, K. Kulangara, F. Guilak and K. W. Leong, *Biomaterials*, 2010, **31**, 1299-1306.
46. C. Li, C. Vepari, H. J. Jin, H. J. Kim and D. L. Kaplan, *Biomaterials*, 2006, **27**, 3115-3124.
47. M. Shin, H. Yoshimoto and J. P. Vacanti, *Tissue Eng*, 2004, **10**, 33-41.
48. W. Yang, F. Yang, Y. Wang, S. K. Both and J. A. Jansen, *Acta Biomater*, 2013, **9**, 4505-4512.
49. Y. Takahashi and Y. Tabata, *J Biomat Sci-Polym E*, 2004, **15**, 41-57.
50. M. J. Dalby, N. Gadegaard, R. Tare, A. Andar, M. O. Riehle, P. Herzyk, C. D. Wilkinson and R. O. Oreffo, *Nat Mater*, 2007, **6**, 997-1003.
51. N. S. Hwang, S. Varghese, H. J. Lee, Z. Zhang and J. Elisseeff, *Tissue engineering. Part A*, 2013, **19**, 1723-1732.
52. B. Bai, J. He, Y. S. Li, X. M. Wang, H. J. Ai and F. Z. Cui, *Biomed Res Int*, 2013, **2013**, 361906.
53. B. K. Teo, S. T. Wong, C. K. Lim, T. Y. Kung, C. H. Yap, Y. Ramagopal, L. H. Romer and E. K. Yim, *ACS Nano*, 2013, **7**, 4785-4798.
54. T. Ozdemir, L. C. Xu, C. Siedlecki and J. L. Brown, *Integr Biol (Camb)*, 2013, **5**, 1407-1416.
55. J. de Boer, R. Siddappa, C. Gaspar, A. van Apeldoorn, R. Fodde and C. van Blitterswijk, *Bone*, 2004, **34**, 818-826.
56. R. M. Salasnyk, R. F. Klees, A. Boskey and G. E. Plopper, *Journal of cellular biochemistry*, 2007, **100**, 499-514.
57. C. Galli, G. Passeri, F. Ravanetti, E. Elezi, M. Pedrazzoni and G. M. Macaluso, *J Biomed Mater Res A*, 2010, **95**, 682-690.
58. X. Liao, S. Lu, Y. Wu, W. Xu, Y. Zhuo, Q. Peng, B. Li, L. Zhang and Y. Wang, *PloS one*, 2013, **8**, e72233.
59. B. Xu, Y. Ju and G. Song, *J Biosci Bioeng*, 2013.
60. S. I. Ertel and J. Kohn, *J Biomed Mater Res*, 1994, **28**, 919-930.
61. Z. M. Huang, Y. Z. Zhang, M. Kotaki and S. Ramakrishna, *Compos Sci Technol*, 2003, **63**, 2223-2253.
62. A. L. Carlson, C. A. Florek, J. J. Kim, T. Neubauer, J. C. Moore, R. I. Cohen, J. Kohn, M. Grumet and P. V. Moghe, *Faseb J*, 2012, **26**, 3240-3251.
63. W. C. Wang, C. Y. Kuo, B. S. Tzang, H. M. Chen and S. H. Kao, *J Cell Biochem*, 2012, **113**, 3567-3575.
64. S. K. Lim, M. Orhant-Prioux, W. Toy, K. Y. Tan and Y. P. Lim, *Faseb J*, 2011, **25**, 3004-3018.